Advances in Magnetic Resonance

NMR studies of protein structure and dynamics

Lewis E. Kay*

Contribution from the Protein Engineering Network Centers of Excellence and the Departments of Medical Genetics, Biochemistry and Chemistry, The University of Toronto, Toronto, Ont., Canada M5S 1A8

Abstract

Recent advances in solution NMR spectroscopy have significantly extended the spectrum of problems that can now be addressed with this technology. In particular, studies of proteins with molecular weights on the order of 100 kDa are now possible at a level of detail that was previously reserved for much smaller systems. An example of the sort of information that is now accessible is provided in a study of malate synthase G, a 723 residue enzyme that has been a focal point of research efforts in my laboratory. Details of the labeling schemes that have been employed and optimal experiments for extraction of structural and dynamics information on this protein are described. NMR studies of protein dynamics, in principle, give insight into the relation between motion and function. A description of deuterium-based spin relaxation methods for the investigation of side chain dynamics is provided. Examples where millisecond (ms) time scale dynamics play an important role and where relaxation dispersion NMR spectroscopy has been particularly informative, including applications involving the membrane enzyme PagP and mutants of the Fyn SH3 domain that fold on a ms time scale, are presented.
© 2004 Elsevier Inc. All rights reserved.

1. Introduction

An impressive number of advances in biomolecular NMR spectroscopy have been reported in the past decade [1–3]. New instrumentation, sophisticated experiments and the development of molecular biology tools for the production of sufficient quantities of the appropriately labeled samples have all played important roles in establishing NMR at the forefront of modern structural biology. In particular NMR has emerged as a powerful probe for the study of protein structure [4–6] and dynamics [7,8], areas that have been the focal point of research efforts in my laboratory for the past decade. In this review of work emanating from my research group I will describe two areas of study that are cur-

rently of great interest. The first deals with the development of experimental tools for NMR structural studies of high-molecular-weight proteins and the subsequent application of this methodology to interesting problems in biochemistry. Studies of the 82 kDa monomeric enzyme malate synthase G (MSG) [9] have been at the forefront of our efforts in this regard and this protein has served as an excellent test-case. A second major area involves using NMR spectroscopy to study molecular dynamics over a wide range of time scales. In particular, the goal is to relate function to dynamics and to study the kinetics, thermodynamics, and structures of weakly populated protein states that are thought to play an important role in function. These two areas of study are very much related from a purely technical perspective, since they both depend on (or are influenced by) spin relaxation. In the case of structural studies of large proteins, the sensitivity and resolution of experiments

* Fax: +1 416 978 6885.
  E-mail address: kay@pound.med.utoronto.ca.

are degraded by extremely rapid transverse relaxation. New methods have emerged that exploit the relaxation properties so as to extend the size-limit for NMR investigations [10]. Similarly, dynamics experiments also make use of relaxation, in this case as a 'spy' of molecular motion [11]. In what follows, aspects of our research in these areas are highlighted, without any attempt to be comprehensive. The interested reader is referred to a number of recent reviews that describe some of this work in more detail [12,13] and that make reference to the appropriate original literature.

2. NMR studies of high-molecular-weight proteins: an application to MSG

2.1. Backbone chemical shift assignments

Fig. 1 illustrates what can be understood as the 'size problem' in biomolecular NMR. A series of proteins are shown, ranging from relatively small molecules, by current standards, to large systems. In applications involving systems as large as 40–50 kDa the rules of the game are well established, both in terms of labeling strategies and the experiments to be performed [14,15], and NMR-derived structures of proteins with molecular weights up to 40 kDa have now been reported [16,17]. In the case of proteins that are significantly larger than this limit it is less clear what the optimal labeling scheme and the necessary experiments for obtaining structural and dynamics information might be. Our initial experiments with MSG, working with an unligated form of the protein, focussed on a perdeuterated, ^{15}N, ^{13}C labeled protein which was unfolded/refolded during a final step in the purification process to restore the full complement of proton spins to the labile amide sites. Remarkably,
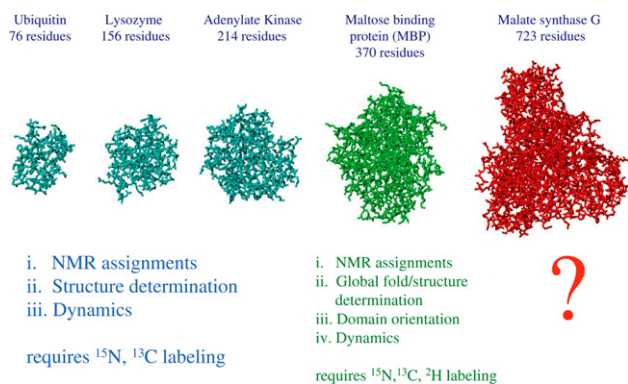
a series of 4D TROSY-based triple-resonance experiments recorded on this sample, supplemented with a 4D NOE data set connecting proximal amide protons, was sufficient to assign over 95% of the backbone ^{1}HN, ^{15}N, ^{13}C$^\alpha$, ^{13}CO, and side chain ^{13}C$^\beta$ spins [18].

The backbone chemical shift assignments served as a starting point for studies of the structure, dynamics and binding properties of the enzyme. Malate synthase G catalyzes the condensation of glyoxylate with acetyl-CoA to produce malate [9]. There is a substantial body of evidence based on structurally and functionally related enzymes suggesting that significant changes in the relative orientation of the four domains of the protein could accompany ligand binding [19,20]. The development of methods to measure residual dipolar couplings resulting from the weak alignment of solute proteins in dilute solutions of ordering media such as bicelles or phage [21,22] allowed us to test this idea. Fig. 2 shows the X-ray derived structure of the glyoxylate bound form of the enzyme [9] (an X-ray structure of the apo-form of the protein was not available at the time of the study) along with correlation plots of measured one-bond ^{1}HN–^{15}N dipolar couplings ($^1D_{NH}$) in each domain and values estimated using the crystal structure as a model for the protein in solution. The strong correlation between measured and predicted couplings indicates that the intra-domain structures are the same for the apo-form of the enzyme in solution (which is the primary focus of our studies) and the glyoxylate-bound crystal state [23]. In addition to information about intra-domain structure, the relative orientation of

Fig. 1. The 'size problem' in solution NMR studies of proteins. Proteins ranging from 76 to 723 residues are included, along with the labeling strategy that is frequently used for each class size and the type of information that is available from standard NMR experiments. Coordinates are obtained from PDB entries 1ubi, 102l, 1ake, 1dmb, and 1d8c for ubiquitin [72], lysozyme [73], adenylate kinase [74], maltose binding protein [75], and malate synthase G [9], respectively.
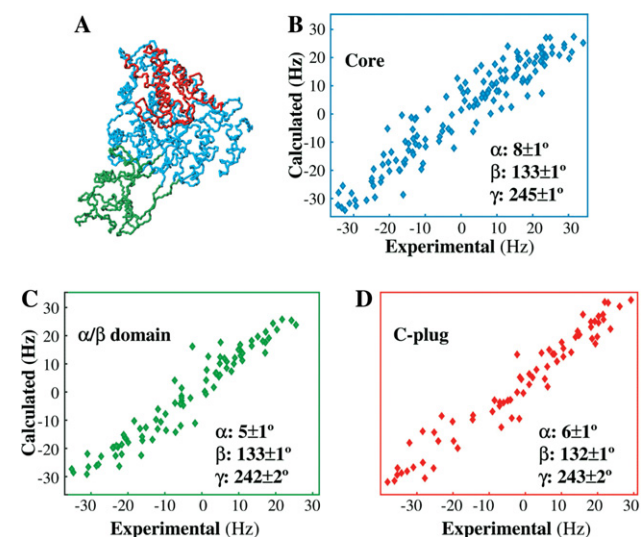

Fig. 2. Using dipolar couplings to orient domains in MSG. (A) X-ray derived structure of the glyoxylate bound form of MSG [9]. (B–D) Correlation plots of measured ^{1}HN–^{15}N dipolar couplings for individual domains in the apo form of MSG and dipolar couplings calculated from a fit of the data using the X-ray structure. Euler angles describing the transformation from the PDB frame (X-ray structure) to the alignment frame are listed. Adapted from Tugarinov and Kay [23].

domains is also obtained via a set of Euler angles, derived from the $^1D_{NH}$ couplings, that effectively describe the transformation of each of the domains from the X-ray to the solution conformation. These angles are the same to within error for each domain, indicating that the relative domain orientations in the crystalline and the apo solution states are identical. It is worth emphasizing that this combined X-ray/NMR analysis can be done rapidly once backbone assignments for a protein are available [24,25]. The complementarity between the two techniques, whereby high-resolution structures of individual domains based on crystallography are combined with domain orientations derived from NMR, is readily apparent.

In addition to studies of domain orientation in MSG, the binding of ligands has also been investigated [23]. The kinetic and thermodynamic parameters measured for the binding process have been supplemented by ^{15}N spin relaxation experiments to provide a picture of how the protein internal dynamics change upon ligand binding. It is clear that the sort of quantitative information that is normally associated with NMR studies of small biomolecules can, at least in some cases, be obtained in high-molecular-weight proteins, when pulse schemes are modified to reflect the challenges associated with the increased size of the system.

2.2. Assignment of methyl groups in MSG

The assignment of backbone chemical shifts allowed us to examine a number of structural and dynamic properties of MSG, however additional assignments were necessary if further structural work was to be undertaken. Structural studies of proteins generally rely on large numbers of distance restraints in the form of proton NOEs [26]. In this regard, the labeling strategy that had been employed so effectively for the assignment of the backbone chemical shifts of MSG (perdeuteration) was a liability since the only protons available for measuring distances were those from labile amide groups. Several years ago our laboratory developed a protocol for the production of Ile (δ1), Leu, Val methyl protonated, highly deuterated proteins using a pair of metabolic precursors, α-ketoisovalerate and α-ketobutyrate, that are added to the growth media prior to protein induction [27,28]. These compounds are now available commercially with a variety of different labeling patterns, and have successfully been used in a number of laboratories. The precursors that were employed in applications involving MSG, along with a ^1H–^{13}C HMQC spectrum of the resulting ^{15}N, ^{13}C, perdeuterated, methyl protonated protein, are shown in Fig. 3. Because protonation is restricted to methyl groups, only the methyl region is observed in the data set; it can be verified that only $^{13}CH_3$ isotopomers are present. Close to 276 methyl cross-peaks can be counted from the 44
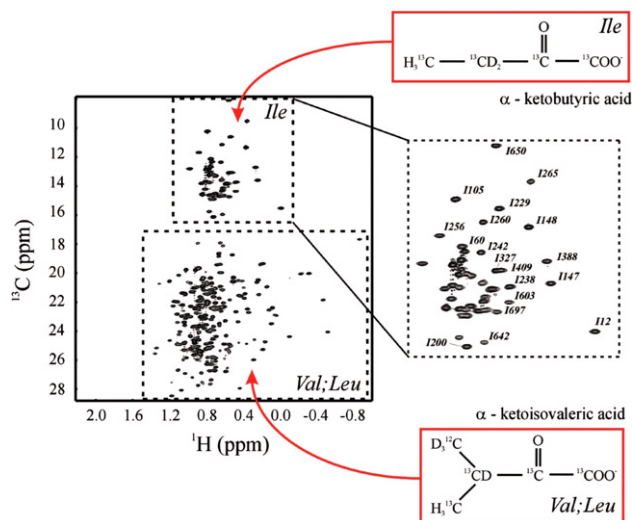

Fig. 3. ^1H–^{13}C CT-HMQC correlation map of U-[^2H,^{15}N,^{13}C]Ileδ1-[$^{13}CH_3$]Leu,Val-[$^{13}CH_3$,$^{12}CD_3$]-labeled-MSG, 800 MHz, 37 °C recorded with a 28 ms constant-time period. The protein was labeled with the precursors shown on the right. Reprinted from Tugarinov and Kay [29], with permission.

Ile, 46 Val, and 70 Leu residues in the protein. It is noteworthy that the variant of isovalerate that was employed for labeling is one where only a single methyl of the pair is of the $^{13}CH_3$ variety, with the second $^{12}CD_3$ [29], for reasons discussed below.

Conventional approaches for the assignment of methyl ^1H and ^{13}C chemical shifts involve the use of TOCSY-based spectroscopy, whereby magnetization that originates on the methyl spins is relayed via the ^{13}C–^{13}C scalar coupling network along the side chain to the backbone amide spins [6]. Because the backbone chemical shifts are available from previous experiments, the correlation of side chain with backbone shifts provides a straightforward way to assign the side chains. This methodology was not successful in applications to MSG [30]. The difficulty lies in the fact that Ile, Leu, and Val are all branched amino acids and subsequently at the branch point there are two pathways of magnetization transfer, with only one of the paths leading to backbone nuclei. As a consequence, 60% of the signal is lost relative to the case where the non-productive pathway is eliminated [30]. In studies of small proteins where the sensitivity is high, inefficiencies of this sort can be tolerated, but not in the case of an 80 kDa molecule. A solution to the problem was developed for Ile by recognizing that the carbon spins at the branch point have well resolved chemical shifts so that it is possible to 'steer' the magnetization to the backbone using a set of COSY magnetization transfer steps together with selective pulses at key points in the pulse scheme [30]. In the case of Leu and Val the pair of methyls resonate at similar positions so that such a scheme is not possible and it was therefore necessary

to resort to chemistry to remove the undesired magnetization transfer pathway [29].

Fig. 4 illustrates the COSY-transfer steps that are used for the assignment of Val methyl groups, along with planes from the 3D data set correlating backbone amide shifts with either methyl ^{13}C (Fig. 4A) or ^{1}H (Fig. 4B) resonance frequencies. The twofold ambiguity associated with linking ^{1}H and ^{13}C chemical shifts to a particular methyl group is resolved using a high-resolution 2D ^{1}H, ^{13}C HMQC, Figs. 4C and D. Note that only a single magnetization transfer path is now available, Fig. 4. Although a factor of two in sensitivity is forfeited (since only one of the two methyls per Leu/Val is spectroscopically active), the gain in signal-to-noise resulting from the linearization of the side chain spin system more than compensates. Close to 90% of the methyls from Ile and Val residues could be assigned from data sets recorded with schemes utilizing a net transfer of magnetization from methyls to amides, however, a significantly smaller fraction (55%) of Leu methyl groups could be assigned using this strategy [29]. As a consequence, a much more sensitive 'out-and-back' experiment was developed, Fig. 5, which correlates aliphatic or carbonyl carbon shifts with those of the methyl spins. This sequence produces data sets that are of much higher sensitivity than those from the methyl-amide experiment since, in the latter scheme it is not possible to effectively transfer magnetization from all three methyl protons, while all contribute fully to the detected signal in the

Fig. 5. 'Out-and-back' approach for assignment of methyl groups in proteins. The top panel illustrates the flow of magnetization in the experiments. Selected ^{13}C^{aliphatic}–^{1}H^{methyl} and ^{13}CO–^{1}H^{methyl} strips from data sets recorded on a U-[^{2}H,^{15}N,^{13}C]Ileδ1-[^{13}CH$_3$]Leu,Val-[^{13}CH$_3$,^{12}CD$_3$]-labeled-MSG sample, 800 MHz, 37 °C, extracted at ^{13}C^{methyl} chemical shifts of I200, L526, and V581 are illustrated, in the middle and bottom panels, respectively. Correlations in black and red are of opposite phase. Adapted from Tugarinov and Kay [29].
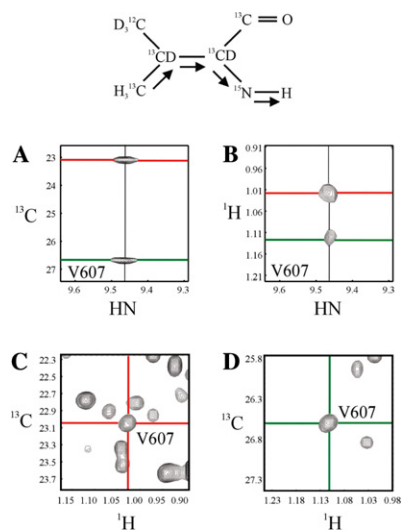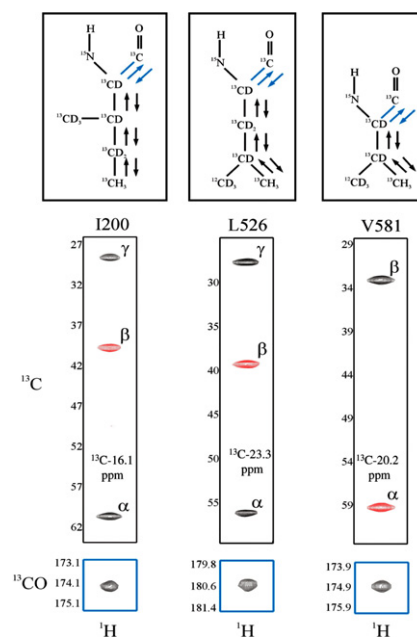

Fig. 4. Methyl-HN COSY assignment strategy. The flow of magnetization is indicated for a Val residue, labeled as described in the text, along with selected regions from ^{13}C^{methyl}–^{1}HN (A) and ^{1}H^{methyl}–^{1}HN (B) planes of 3D data sets extracted at the ^{15}N chemical shift of Val 607, MSG. The ^{13}C^{methyl} and ^{1}H^{methyl} chemical shifts are linked via high-resolution 2D HMQC data sets, as indicated in (C) and (D) using red and green cross-hairs. Data recorded on a U-[^{2}H,^{15}N,^{13}C]Ileδ1-[^{13}CH$_3$]Leu,Val-[^{13}CH$_3$,^{12}CD$_3$]-labeled-MSG sample, 800 MHz, 37 °C. Adapted from Tugarinov and Kay [29].

'out-and-back' version. Also it avoids the costly transfer step from the backbone carbon (typically ^{13}C$^\alpha$ for applications at high-magnetic fields or ^{13}CO for studies of smaller proteins) which can be limiting. Combining data from the two types of experiments described above led to the assignment of 95, 91, and 99% of the Ile, Leu, and Val methyls in MSG [29].

2.3. Methyl TROSY spectroscopy

The relaxation properties of methyl groups can be complex [31–34]. The availability of nearly complete methyl chemical shift assignments in MSG heightened our interest in exploring whether this complexity could be exploited to enhance both the resolution and the sensitivity of experiments that make use of methyls as probes of molecular structure and dynamics. Fig. 6 show an energy level diagram of an isolated ^{13}CH$_3$ spin system with the ^{1}H (vertical arrows) and ^{13}C (horizontal arrows) single quantum transitions highlighted. In general, longitudinal and transverse relaxation is decidedly multi-exponential, due largely to ^{1}H–^{13}C dipolar cross-correlated spin interactions. In the case of an isolated methyl attached to a macromolecule it can be shown that the relaxation of each of the single quantum transitions is mono-exponential, so long as the methyl group rotates rapidly about its threefold axis
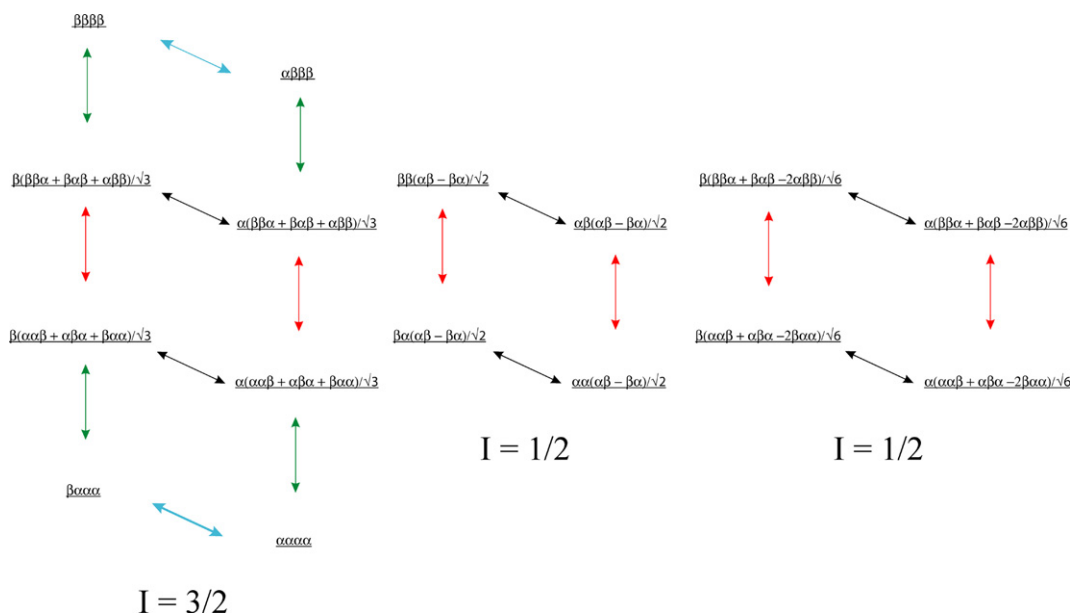
Fig. 6. Energy level diagram for an isolated $^{13}CH_3$ spin system with wave functions written in an irreducible basis representation. The first spin state in each function corresponds to the ^{13}C spin, with the remaining associated with the ^1H spins. The total spin angular momentum of each manifold is listed along with the ^1H transitions (vertical lines; green and red corresponding to fast and slowly relaxing transitions) and ^{13}C transitions (horizontal lines; blue and black indicate fast and slowly relaxing transitions). Adapted from Tugarinov et al. [36].

[35]. Furthermore, each line relaxes with either a fast (green, blue) or a slow (red, black) rate. This situation is reminiscent of the effect that occurs in isolated ^1HN–^{15}N spin pairs due to interference between dipolar and CSA interactions that has been exploited very cleverly by Pervushin et al. [10] in the development of TROSY spectroscopy. Could a similar approach be applied to methyl groups?

Our initial attempts to construct a pulse scheme that would isolate slow from fast relaxing methyl coherences failed and only when an HMQC experiment was examined did we understand why [36]. Fig. 7 shows an HMQC pulse scheme with the ^1H 180° pulse that is normally positioned in the center of the t_1 period removed to illustrate the essential features of methyl-TROSY. (It is worth emphasizing that the ^1H pulse is removed only for the purpose of illustration; all methyl-TROSY experiments make use of an F_1-decoupled experiment recorded using a standard HMQC sequence [37,38]). In the present description we consider an isolated methyl group with the methyl protons on resonance. At position a in the pulse scheme the coherence of interest is proportional to $I_X C_Y$, where I_X and C_Y are the X- and Y-components of ^1H and ^{13}C magnetization, respectively. Focussing for the moment only on the multiple quantum term associated with proton spin 1 (denoted by $I_X^1 C_Y$) it is shown in the figure that there are three components that evolve separately due to the coupling between C and protons 2 and 3, each separated by J_{CH} Hz. In the absence of differential relaxation, a 1:2:1 triplet in the ^{13}C dimension (F_1)

results. A simple local field argument establishes that each of the lines should in fact relax quite differently for a methyl rotating rapidly in a macromolecule, because the dipolar fields due to protons 2 and 3 are additive in the case of the outer lines, while for the inner line they cancel. Indeed, a more rigorous treatment shows that the inner line does not relax at all from intra-methyl dipolar interactions [36]. This is illustrated by a comparison of experimental data recorded on sodium acetate (Fig. 8A) and a sample of MSG (Fig. 8B) using a sequence which selects ^1H–^{13}C double-quantum coherences during t_1. For sodium acetate a triplet with line intensities that are close to the expected 1:2:1 ratio is observed while for U-[^2H,^{15}N]Ileδ1-[$^{13}CH_3$]-labeled-MSG, 37 °C (correlation time, τ_C, of 45 ns) it is clear that the outer lines relax much more rapidly than the inner component. Application of a ^1H 180° pulse in the center of t_1, as would normally be done, interconverts the outer lines without mixing the outer and center components so that the slow relaxation of the middle line is preserved.

In addition to the differential relaxation of the multiplet components associated with multiple quantum coherences that evolve during t_1, ^1H coherences that are present during the remainder of the sequence of Fig. 7 also relax very differently. A detailed analysis of the flow of coherence through the HMQC sequence shows that slowly relaxing proton transitions are converted to slowly relaxing multiple quantum coherences and then back to slowly relaxing proton transitions for detection [36]. A parallel pathway involving only fast
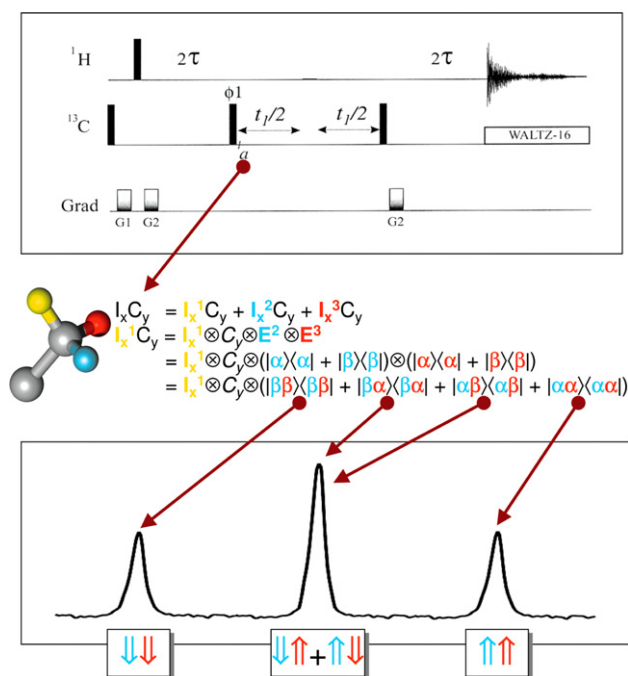
Fig. 7. HMQC spectroscopy of a methyl group. An HMQC pulse scheme is illustrated with the ^1H 180° pulse in the center of the t_1 period omitted (for illustrative purposes only) and the resultant F_1 trace indicated below. The relevant product operator at point a in the scheme is shown. Each of the multiple quantum terms associated with the methyl ^{13}C and one of the three methyl ^1H spins is indicated. The term $I_X^1 C_Y$ is written in terms of direct products of operators of I_X^1 and C_Y, along with identity operators E^2 and E^3, corresponding to proton spins 2 (blue) and 3 (red). In this way $I_X^1 C_Y$ can be 'decomposed' into three lines corresponding to protons 2 and 3 in the [down, down], [up, down/down, up] and [up, up] positions. Differential relaxation of the individual lines has not been included.
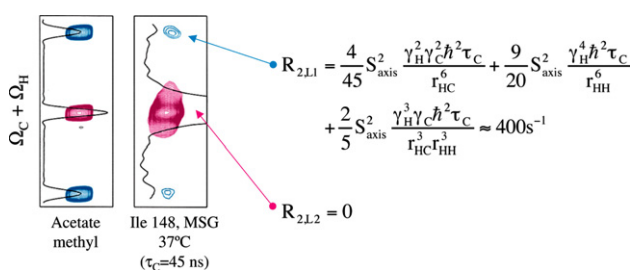

Fig. 8. ^{13}C multiplet structures in ^1H–^{13}C double quantum correlation maps recorded on (A) sodium acetate and (B) U-[^2H,^{15}N]Ileδ1-[$^{13}CH_3$]-labeled-MSG, 800 MHz, 100% D_2O, 37 °C, along with expressions for the relaxation of the outer ($R_{2,L1}$) and inner ($R_{2,L2}$) lines in the macromolecular limit taking into account contributions from intra-methyl dipolar relaxation only. All parameters in $R_{2,L1}$ are defined as in Tugarinov et al. [36], with $R_{2,L1}$ calculated using $\tau_C = 45$ ns, $S_{axis}^2 = 0.5$. Note that in HMQC spectra (i.e., where a ^1H 180° pulse is applied in the center of t_1 so that J evolution is refocused) the third term in the expression for $R_{2,L1}$ is absent and $R_{2,L1} \sim 200$ s^{-1}. Adapted from Tugarinov et al. [36].

relaxing elements (comprising half of the detected signal in the absence of relaxation) is also present, but for applications involving large proteins this pathway

contributes very little to the ultimate signal. The HMQC pulse scheme is therefore completely optimized 'as is' for the TROSY effect. In contrast, pulse schemes that inter-convert fast and slowly relaxing pathways are less efficient. An example is the much more common HSQC [39] that employs several 90° ^1H pulses, effectively mixing fast and slowly relaxing transitions. This is illustrated in Fig. 9 where a comparison of HMQC and HSQC spectra recorded on U-[^2H,^{15}N]Ileδ1-[$^{13}CH_3$] MSG, 5 °C ($\tau_C \sim 120$ ns) is presented. It is now clear why we had been unsuccessful in developing methyl-TROSY experiments in the past; all of our previous sequences contained a number of 90° ^1H pulses.

Like the AX-TROSY experiments, the methyl-TROSY effect is attenuated by neighboring proton spins since cross-relaxation involving protons proximal to the methyl group leads to exchange between transitions that mixes the rapidly and slowly relaxing pathways. This can be minimized by working with samples that are highly deuterated, as in the case of the Ileδ1-[$^{13}CH_3$]-labeled protein discussed above. It is possible to increase the number of probes beyond Ile by preparing molecules that are U-[^2H]Ileδ1-[$^{13}CH_3$]Leu,Val-[$^{13}CH_3$,$^{12}CD_3$]-labeled [40]. Note that this labeling approach eliminates contributions to relaxation that would normally result between methyls from the same residue. Fig. 10 shows a comparison between an HSQC spectrum recorded on a sample of U-[^2H]Leu,Val-[$^{13}CH_3$,$^{13}CH_3$]MSG, 37 °C and an HMQC data set obtained with a U-[^2H]Leu,Val-[$^{13}CH_3$,$^{12}CD_3$]-
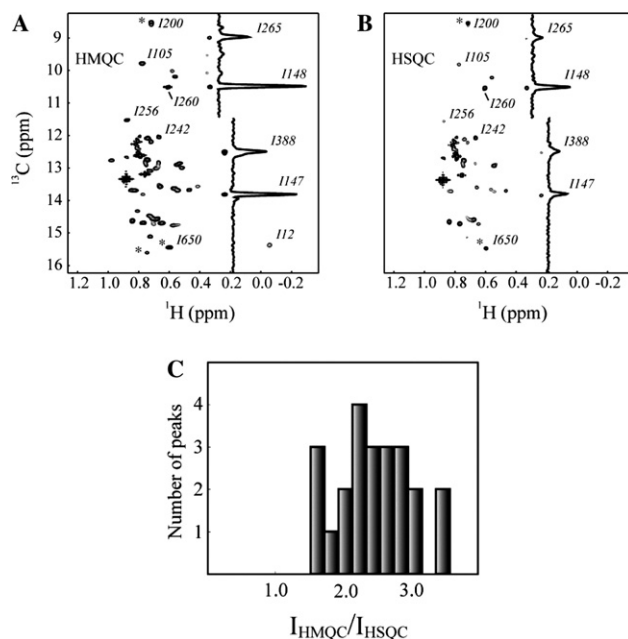
Fig. 9. Comparison of ^1H–^{13}C HMQC (A) and HSQC (B) spectra of U-[^2H,^{15}N]Ileδ1-[$^{13}CH_3$]-labeled-MSG, 800 MHz, 100% D_2O, 5 °C. Each data set is plotted at the same noise-level. An average gain in signal-to-noise of a factor of 2.6 is noted for the HMQC relative to the HSQC (C). Adapted from Tugarinov et al. [36].
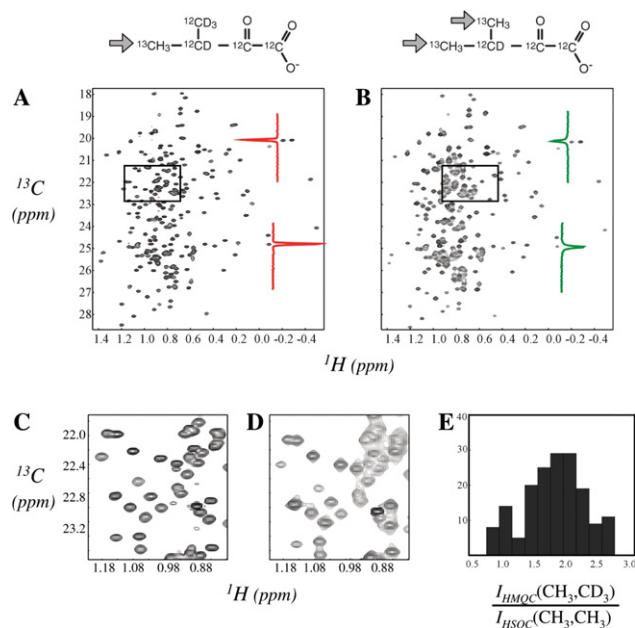
Fig. 10. Comparison of a ^{1}H–^{13}C HMQC spectrum recorded on a U-[^{2}H,^{15}N]Leu,Val-[^{13}CH$_3$,^{12}CD$_3$]-labeled-MSG sample (A) with an HSQC map recorded on U-[^{2}H,^{15}N]Leu,Val-[^{13}CH$_3$,^{13}CH$_3$]-labeled-MSG (B). Data were recorded at 800 MHz, 100% D$_2$O, 37 °C on samples of the same concentration. The precursors used for the labeling are indicated above the correlation maps. Selected regions (C and D) of the data sets in (A and B) illustrating the improvements in resolution and sensitivity (E) associated with methyl-TROSY spectroscopy.

Fig. 11. (A) Schematic representation of a methyl group and neighboring ^{1}H/^{2}H spins. The local dipolar fields from an isolated spin (proton) add in the case of ^{1}H–^{13}C double-quantum (B) and subtract for ^{1}H–^{13}C zero-quantum coherences (C). Red and black arrows denote spin states of methyl ^{1}H and ^{13}C spins that participate in the double/zero quantum transition, with the green arrow indicating the spin state of the proximal external proton. 'HH' and 'HC' denote ^{1}H–^{1}H and ^{1}H–^{13}C dipolar interactions, respectively, involving the external proton and the methyl proton (red) and carbon spins.

labeled sample at the same protein concentration. Despite the fact that the concentration of methyls in the latter sample is half that in the former, the HMQC experiment is clearly superior both in terms of resolution and in terms of sensitivity. Of interest, the gain in signal-to-noise increases to almost 4-fold in a similar comparison of spectra recorded at 5 °C [40].

As described above for an isolated methyl group, the multiple quantum elements that evolve during t_1 in the HMQC and that ultimately contribute to the observed signal in applications involving macromolecules are free of relaxation contributions from intra-methyl dipolar interactions. However, methyl groups are not isolated (Fig. 11A) and indeed spins external to the methyl do cause relaxation; it is important, therefore, to develop experiments that minimize these effects. External spins influence the relaxation of the double- and zero-quantum components of $I_X C_Y$ differently, as illustrated in Figs. 11A and B, and this difference can be exploited [41]. Panels B and C of the figure depict double- and zero-quantum transitions involving methyl spins and show how such transitions relax due to an external proton spin (green). A local field argument establishes that in the macromolecular limit, dipolar interactions involving the external proton and the methyl proton and carbon spins are additive for double-quantum ($I_+ C_+$),
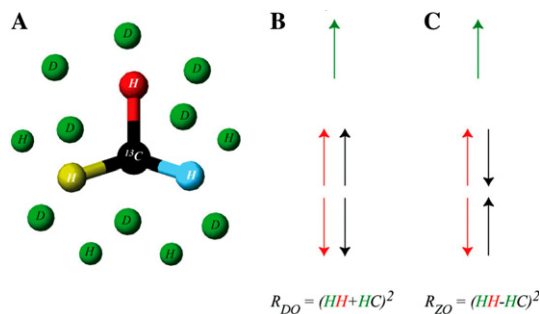
while for zero-quantum ($I_- C_+$) the fields subtract. This effect can be substantial, as illustrated in Fig. 12A, where a comparison of the relaxation rates of $I_X C_Y$ (($R_{DQ} + R_{ZQ}$)/2) and $I_- C_+$ (R_{ZQ}) is given for Ile, Leu and Val residues in U-[^{2}H]Ileδ1-[^{13}CH$_3$]Leu,Val-[^{13}CH$_3$,^{12}CD$_3$]MSG. The ratio of rates is independent of the external magnetic field, as expected for relaxation contributions that are dipolar in origin [36,41], and also independent of correlation time, so long as the overall tumbling remains in the macromolecular limit.
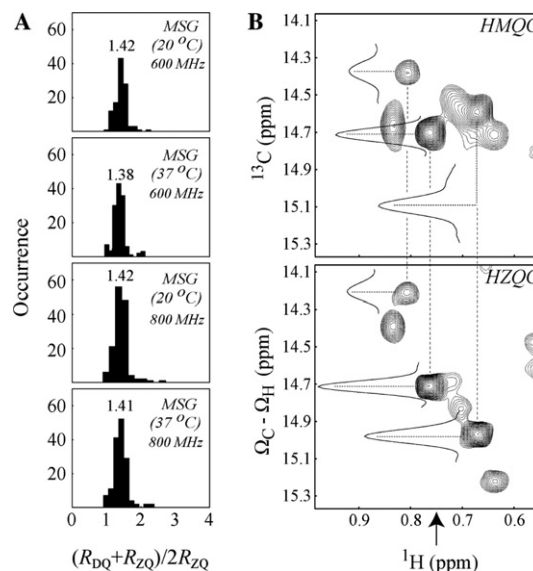

Fig. 12. (A) F_1 linewidths (($R_{DQ} + R_{ZQ}$)/2) in HMQC data sets of MSG are on average 40% larger than in zero-quantum data sets, HZQC (R_{ZQ}), ($R_{DQ} + R_{ZQ}$)/($2R_{ZQ}$)≈1.4. (B) Comparison of Ile region of HMQC and HZQC maps recorded on a U-[^{2}H,^{15}N]Ileδ1-[^{13}CH$_3$]Leu,Val-[^{13}CH$_3$,^{12}CD$_3$]-labeled-MSG sample, 600 MHz, 5 °C. The position of the ^{1}H carrier is indicated with the vertical arrow. Adapted from Tugarinov et al. [41].

Significant gains in resolution in zero-quantum correlation spectra (HZQC) relative to their HMQC counterparts can be obtained, as illustrated in a comparison of the Ile regions of HMQC and HZQC data sets recorded on MSG, Fig. 12B , at the expense of only very slight (~10%) losses in sensitivity [41].

A number of applications involving methyl-TROSY spectroscopy have emerged. HMQC- and HZQC-based quantitative J experiments [42] have been developed to obtain stereospecific assignments of pro-chiral methyls of Val residues [43], along with information about χ_1 torsion angle dynamics. TROSY-based relaxation dispersion experiments have been used to probe millisecond (ms) time scale dynamics in the hydrophobic core of MSG [44], and most recently to study dynamics in a 300 kDa ClpP protease complex. Notably, we have exploited the increased transverse relaxation times of methyl-TROSY coherences to record 3D and 4D ^{1}H, ^{13}C NOE-based experiments with high-resolution in the non-acquisition dimensions, using non-linear sampling schemes [45]. Experiments of this sort have allowed us to obtain a significant number of long range methyl–methyl distance restraints, leading to the de novo determination of the enzyme's global fold.

3. Probing functional protein dynamics

3.1. ^{2}H spin-relaxation studies of protein side chain dynamics

In the previous section, we have shown that the rich network of coupled dipolar interactions that plays a dominant role in the relaxation of methyl spins can be put to good use in a number of important applications involving high-molecular-weight proteins. The multiexponential relaxation behavior that results from the dipolar cross-correlations does, however, present challenges in obtaining dynamics information from heteronuclear (^{13}C) relaxation experiments in a straightforward manner. Experiments of this sort, especially the related ^{15}N versions [46,47], have become very popular for studying protein motions on a picosecond (ps) to nanosecond (ns) time scale. In contrast, schemes for AX_3 spin systems have been less successful and the rates measured are at best semi-quantitative [48].

Several years ago we decided to follow the lead of solid state NMR and use ^{2}H spin relaxation as a probe of ps–ns dynamics in biomolecules. The advantage of using the deuteron to study dynamics is that its relaxation is dominated by the well understood quadrupolar interaction [49]. A major challenge for solution state applications, where the goal is to study large numbers of sites at once, is the need for high-resolution. The poor dispersion of lines (due to the low gyromagnetic ratio of deuterons relative to protons) and the efficient relaxation severely

limits resolution in ^{2}H-detect experiments. With this in mind, a labeling strategy was proposed in which uniformly ^{13}C and fractionally deuterated proteins are prepared with the relaxation properties of the deuteron monitored by the intensities of correlations in well resolved ^{1}H–^{13}C spectra [50]. In the case of methyl groups, the ^{13}CH$_2$D isotopomer is of interest and a magnetization transfer scheme, ^{1}H → ^{13}C → ^{2}H(T) → ^{13}C(t_1) → ^{1}H(t_2), is employed, where only this isotopomer is selected. (In the transfer scheme above T is the time during which ^{2}H relaxation occurs and t_i is an acquisition time). Fig. 13 shows the five different density elements whose relaxation properties can be measured [51,52], along with the corresponding populations/transitions. The fact that five probes of dynamics at each methyl site are available provides an unprecedented opportunity to study side chain dynamics in detail.

Fig. 14 shows a ^{1}H–^{13}C correlation map of a uniformly ^{13}C, fractionally deuterated sample of protein L along with relaxation curves measured for each of the five ^{2}H relaxation rates for Leu 56δ2. It can be shown that the five rates probe the spectral density function, $J(\omega)$, at only three frequencies, 0, ω_D, and $2\omega_D$, where ω_D is the ^{2}H Larmor frequency [49]. The redundancy of the experimental data can be exploited to derive a set of consistency relations that relate linear combinations of measured relaxation rates, R^Q [53]; Figs. 15A and B show that there is excellent agreement between the rates measured for protein L. In addition, so long as the spectral density function decreases with increasing frequency, the relaxation rates are predicted to follow the set of inequalities indicated at the top of Fig. 15C, as is certainly the case for protein L [51].

^{2}H spin relaxation experiments have been applied to a large number of systems. The role of dynamics in molecular recognition [54,55], protein folding [56], protein stability [57], and the response of dynamics to hydrophobic core mutations [58,59] are a number of areas that have been investigated.
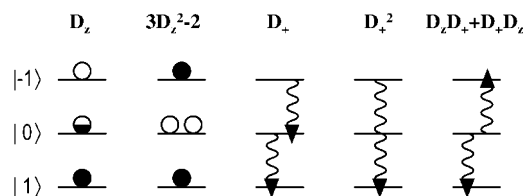

Fig. 13. Five different independent density elements for an isolated ^{2}H spin and the corresponding transitions/populations. (The relaxation properties of each operator are described in Millet et al. [51]) The wave functions for the three ^{2}H Zeeman states are $|{-}1{>}$, $|0{>}$ and $|1{>}$. Populations are indicated by circles (filled circles indicate an excess population, open circles a depleted population and half-circles no excess population relative to a demagnetized, saturated state), while transitions are denoted by wavy arrows. Adapted from Millet et al. [51].
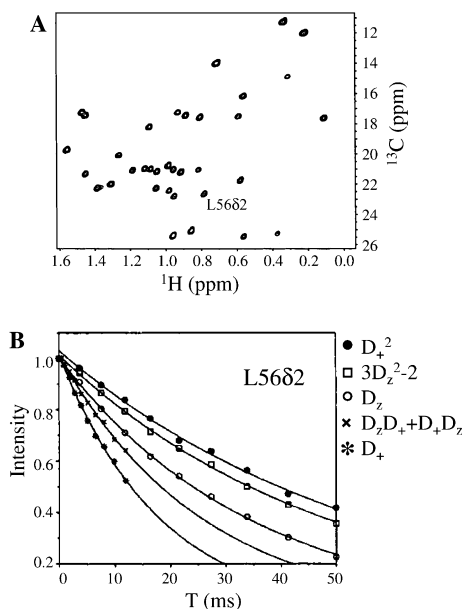
Fig. 14. (A) ^{1}H–^{13}C HSQC map of the methyl region of the B1 domain of peptostreptococcal protein L, 600 MHz 25 °C, recorded using a pulse scheme measuring the decay of ^{2}H double-quantum coherence (D_+^2 in Fig. 13). (B) Decay of the five density elements shown in Fig. 13 for Leu 56δ2.
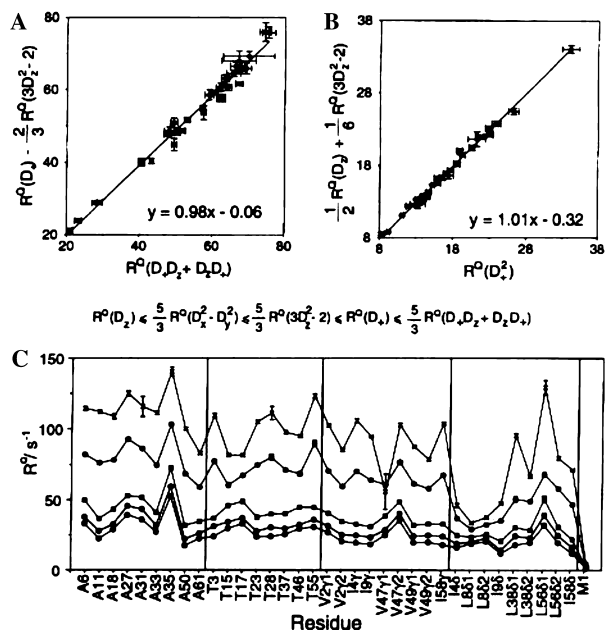

Fig. 15. (A and B) Consistency relations for the five experimentally determined ^{2}H relaxation rates (R^Q)/methyl in protein L, 298 K, 600 MHz. Best fit lines are indicated. (C) Plot of the five measured ^{2}H rates (multiplied by the appropriate factors) as a function of residue in protein L. Note that the system of inequalities indicated at the top of the figure is obeyed for each residue. Adapted from Millet et al. [51].

3.2. An application to the integral membrane enzyme PagP

The leading role that NMR can play in defining the relation between dynamics and function is exemplified

by our studies of PagP [13,60,61]. PagP is an integral membrane enzyme that catalyzes the transfer of the sn-1 palmitate chain from phospholipid to lipopolysaccharide in Gram-negative bacteria [62], Fig. 16A. NMR studies of the enzyme solublized in detergents (that do not support activity) such as dodecylphosphocholine (DPC) or β-octylglucoside (β-OG) showed that the structure is an eight stranded β-barrel [60], Fig. 16B, and notably that many of the putative active site residues (blue in Fig. 16C) are located in a long, highly flexible loop (L1), Fig. 16B. How can enzyme activity be supported in a protein where key residues are highly dynamic?

To address this question we felt that it was necessary to work with an active form of the protein. Fortunately, a subsequent X-ray structure of PagP showed a single detergent molecule bound in the center of the barrel [63]. Guessing that the reason for the lack of activity in the NMR samples was the result of bound detergent as well, we solubilized the enzyme in CYFOS-7, an analogue of DPC with a bulky cyclohexyl group at the terminus of the lipid that prevents penetration into the barrel. Activity of PagP in this new environment was confirmed by monitoring the hydrolysis of substrate by 1D NMR experiments [61].

Initial work on the active form of the protein proceeded at 45 °C, Fig. 17A, and nearly complete
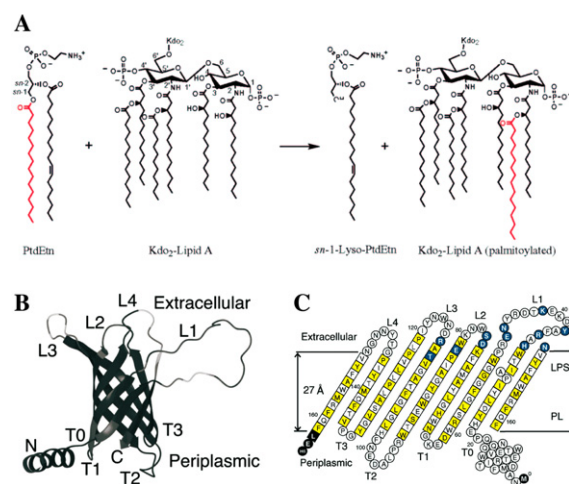

Fig. 16. (A) Reaction catalyzed by PagP in which a palmitate chain (red) from the sn-1 position of a phospholipid, such as phosphatidylethanolamine (PtdEtn) is transferred to lipid A. (B) Ribbon diagram of the NMR-derived solution structure of PagP (DPC) with loops and turns indicated by L and T, respectively. (C) Topology model of PagP showing the positions of the putative active site residues (blue). The membrane is indicated with horizontal lines, with PL and LPS denoting phospholipid (inner leaflet) and lipid A (outer leaflet), respectively. Residues in squares are part of β-strands, residues in yellow squares have side chains facing the membrane bilayer, while white squares indicate side chains lining the interior of the β-barrel. Further details can be found in Hwang et al. [60]. Adapted from Hwang et al. [60].
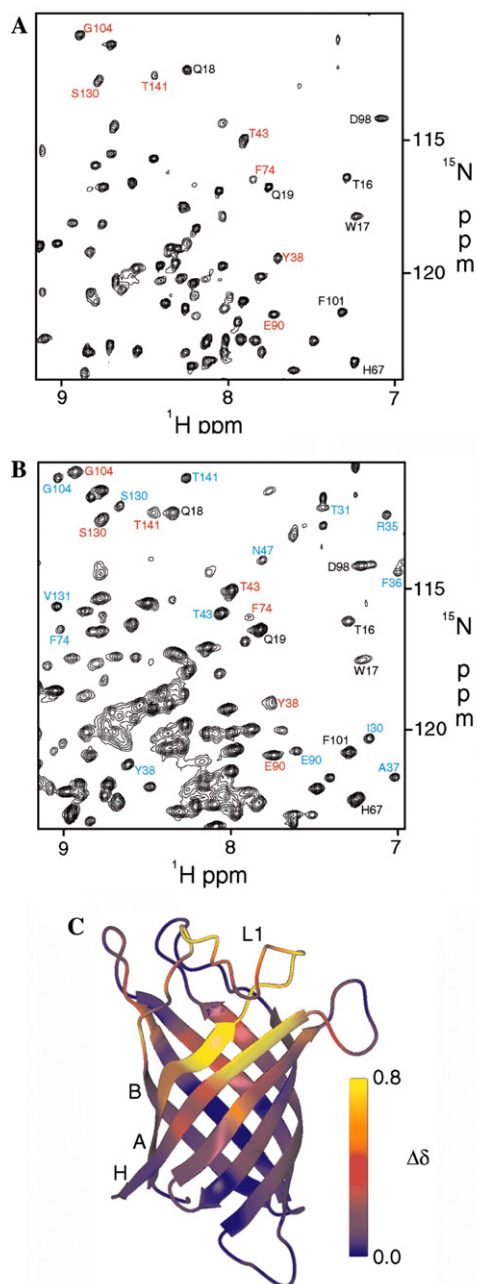
Fig. 17. ^{1}HN–^{15}N TROSY–HSQC spectra of PagP in CYFOS-7, 45 °C (A) and 25 °C (B). Some of the correlations from residues in the R state are labeled in red, with the corresponding T state cross-peaks indicated in blue. Correlations from residues with the same chemical shifts in R and T states are labeled in black. (C) Chemical shift differences between R and T states superimposed on a ribbon diagram of the structure of PagP, $\Delta\delta^{R,T} = \{(\omega_N\Delta\delta_N)^2 + (\omega_{C\alpha}\Delta\delta_{C\alpha})^2 + (\omega_{CO}\Delta\delta_{CO})^2\}^{1/2}$ with $\omega_N = 0.154$, $\omega_{C\alpha} = 0.276$ and $\omega_{CO} = 0.341$. Adapted from Hwang et al. [61].

backbone assignments were obtained. Notably, the chemical shift assignments of the protein in CYFOS-7 were essentially identical to those obtained for the inactive enzyme in either DPC or β-OG at this temperature. Upon lowering the temperature to 25 °C the ^{1}HN–^{15}N correlation map deteriorated significantly with many

of the cross-peaks significantly broadened, Fig. 17B. Remarkably, it was still possible to obtain backbone assignments for the great majority of residues and it became clear from the analysis that two sets of cross-peaks were present [61]. A first set of shifts, derived from what we refer to as the R-state of the enzyme, is identical to the only set observed at 45 °C, and a new set (from the T-state) shows extensive changes in chemical shifts for some residues (for example *F*74, Fig. 17B). The differences in shifts between the R and T states are summarized in Fig. 17C, establishing that there are significant structural differences between the two forms of the enzyme in the L1 loop and in strands βA and βH that are proximal to the loop. Notably, the chemical shifts of the R state in this region are in good agreement with those measured for unstructured peptides.

The exchange between R and T states can be quantified in cases where both sets of correlations are observed (i.e., at temperatures lower than about 35 °C) by recording a series of experiments in which the exchange is monitored via the time dependence of longitudinal nitrogen magnetization during a mixing period [64]. Fig. 18A shows portions of spectra, including cross-peaks for Ser130 and Arg158, recorded with a mixing time of 142 ms; the intense (diagonal) correlations are those that are present in a regular HSQC, while the additional cross-peaks result from the transfer of magnetization between states due to the exchange process. The buildup of these exchange peaks can be fit simultaneously with the decay of the diagonal correlations to extract rates of interconversion. At 25 °C the average values for the R → T (k_{RT}) and T → R (k_{TR}) rates are 2.8 ± 0.5 and 6.5 ± 0.9 s^{-1}, respectively, so that the fractional population of the T state is ~0.3. At higher temperatures only a single set of correlations is observed (from the R state) and exchange kinetics are best obtained through a series of relaxation dispersion experiments [65], Fig. 18B. Here, ^{15}N relaxation rates, $R_{2,\,eff}$, are measured as a function of the number of refocusing pulses, separated in time by $(2\,\nu_{CPMG})^{-1}$, that are applied in a constant-time element of an HSQC pulse scheme. Dispersion profiles, recorded at 600 and 800 MHz fields, are fit to a set of equations derived for a two-site exchange model so that rates, populations and differences in chemical shifts between exchanging states can be extracted. Values of $k_{RT} = 33$ s^{-1} and $k_{TR} = 298$ s^{-1} are obtained, corresponding to a T state population of 10%, 45 °C. Moreover, values of shift changes are in good agreement with differences in shifts at lower temperatures where R and T states are both observed, confirming that the exchange process at 45 °C is indeed the R,T interconversion.

In addition to measuring the kinetic parameters at 25 and 45 °C, the R,T equilibrium constant has been quantified as a function of temperature from which the enthalpy and entropy changes for the T to R conversion
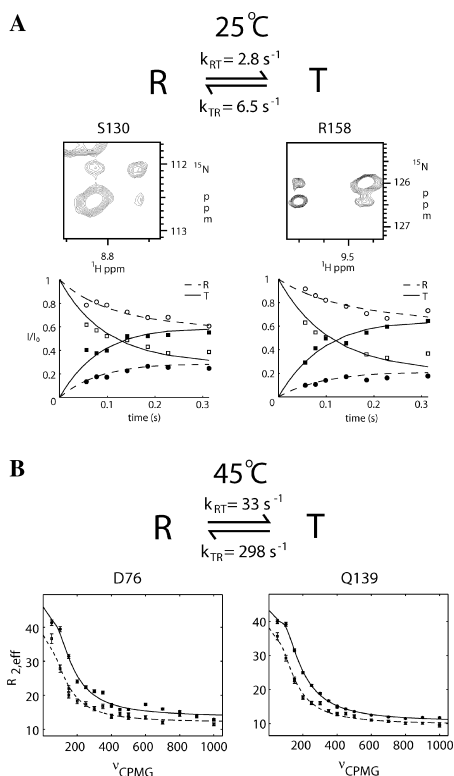
Fig. 18. R,T interconversion measured by ^{15}N magnetization exchange spectroscopy, 25 °C (A) and ^{15}N relaxation dispersion spectroscopy, 45 °C (B). In (A) portions of ^{1}HN–^{15}N correlation maps are shown with peaks at $(\omega_N^{R,T}, \omega_H^{R,T})$, corresponding to 'regular' HSQC correlations and at $(\omega_N^{R,T}, \omega_H^{T,R})$, from the transfer of magnetization between R and T conformers during a mixing time. The decay of auto- and buildup of transfer-peaks are indicated with open and closed symbols, respectively, for Ser 130 and Arg 158. The curves are normalized so that the starting intensities of the auto-peaks are 1 for both R and T states. In (B) dispersion profiles for Asp 76 and Gln 139 are shown, recorded at 800 MHz (circles) and 600 MHz (squares). The solid (800 MHz) and dashed (600 MHz) lines indicate best fits to the experimental data points assuming a two-site exchange process. Errors are indicated with vertical lines through the points. Adapted from Hwang et al. [61].

can be obtained, $\Delta H = 10.7$ kcal/mol, $\Delta S = 37.5$ cal/mol·K. The enthalpy/entropy compensation is consistent with a local unfolding process (T → R) that is localized to residues in the vicinity of the L1 loop (since this is the region that shows the exchange).

The picture that emerges is one where PagP interconverts between a dynamic state (R) that allows substrate entry and a more rigid state (T) in which active site residues from the L1 loop are repositioned to support catalysis. Despite the size of the complex (effective molecular weight of 50–60 kDa) and the fact that the T state is populated at a level of only 30% at 25 °C, both structural and dynamic information on both states have been obtained [61]. A model for the role of motion in this system has been proposed [61] and experiments are currently in progress to test it further.

3.3. NMR studies of protein folding

One of the outstanding problems in structural biology is how the sequence of amino acids in a protein encodes its three-dimensional structure [66]. NMR spectroscopy is particularly well suited to address this important question because it can be used to probe structure in highly dynamic systems and because site specific probes of the formation or dissolution of structure are available through, for example, hydrogen exchange experiments [67].

Our interest in protein folding dates back over a decade to collaborative studies of the N-terminal SH3 domain of the *Drosophila* signaling adapter protein, drk [68]. More recently we have been studying a number of mutants of an SH3 domain from the Fyn tyrosine kinase [69,70]. These mutants, in which a Gly at position 48 is replaced by residues such as Met, Leu, Val or Ile, fold and unfold with exchange rates on the order of 200–1000 s^{-1} and have stabilities ~2 kcal/mol, so that the unfolded state is populated at a level of a few percent. The kinetics and thermodynamics of this system are ideally suited for relaxation dispersion experiments that probe slow (ms) time scale dynamics in biomolecules.

Fig. 19A highlights the site of mutation in the structure of the wild-type Fyn SH3 domain [71]. Dispersion curves probing the contribution to the backbone amide ^{15}N linewidth from the unfolding/folding reaction are shown in the inset to Fig. 19B for Ala 12. On a per-residue basis, the profiles are well fit to a simple kinetic scheme involving two states (F, folded and U, unfolded) and the extracted parameters are very similar to those obtained from stopped flow fluorescence experiments that probe the folding process [70]. The distinguishing feature of NMR over other spectroscopic techniques that monitor average properties or that study only a single site is that every backbone amide can be queried to obtain information about the folding process. The importance of site-specific data is made clear in Fig. 19B where folding (k_f) and unfolding (k_u) rates are plotted for a number of sites in the G48M mutant. These rates have been obtained from fits of dispersion data to a two-state model of exchange (U ↔ F) and all values of k_f (and similarly k_u) are expected to be the same if this model is correct. Although the rates converge at high-temperature, at 15 °C there is an order-of-magnitude difference between k_f values obtained for individual sites, arguing strongly that the folding reaction is more complex than two-state [70].

The dispersion data can be well fit to a three-state model (U ↔ I ↔ F), where an intermediate state (I) is included in the analysis, Fig. 19C. Here, four global parameters are employed, k_{UI}, k_{IU}, k_{IF}, and k_{FI}, along with local parameters, such as differences in chemical
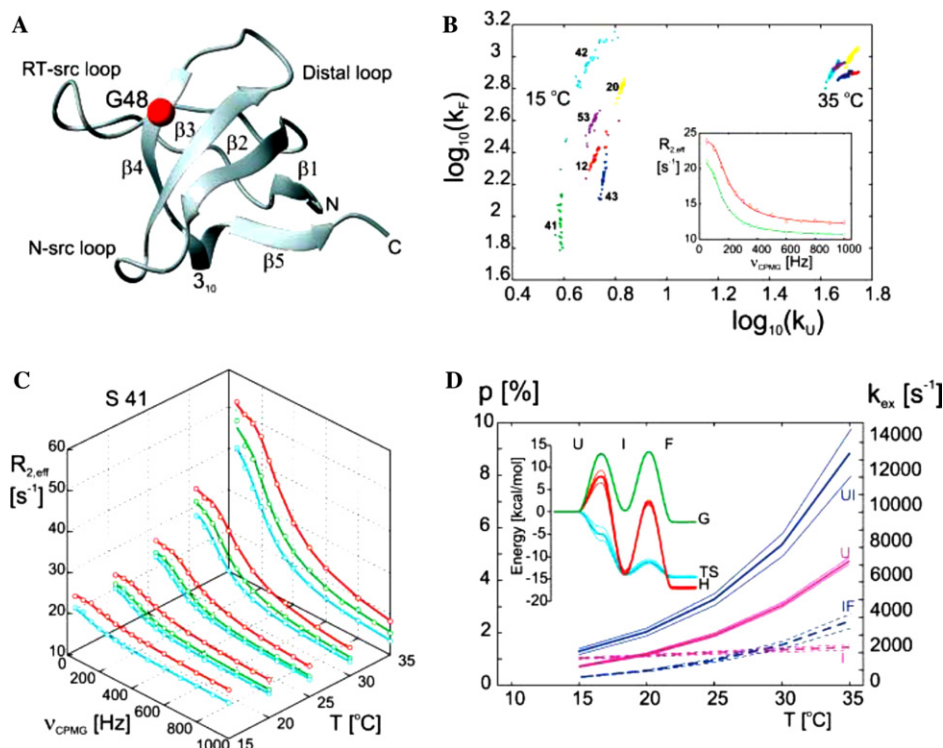
Fig. 19. (A) Ribbon diagram of the wild-type Fyn SH3 domain (pdb accession code 1SHF [71]), highlighting position 48 that has been mutated. (B) Folding (k_f) and unfolding (k_u) rates for selected residues in G48M, indicated by residue number, at 15 and 35 °C. Rates were obtained by fitting dispersion profiles on a per residue basis using a two-site exchange model, with errors estimated using a jacknife procedure whereby 25% of the points in each dispersion were randomly removed and the fits repeated. The inset shows a pair of ^{15}N dispersion profiles recorded at 800 (red) and 600 MHz (green) for Ala 12. The theoretical curves predicted by a two-site exchange model and fitted exchange parameters are shown as solid lines (fits to Ala 12 only). (C) Fits of ^{15}N relaxation dispersion data for Ser 41 (G48M) to a global three-site folding model. Data recorded at 800, 600, and 500 MHz are indicated with red, green and blue circles, respectively, while the best fit is denoted by the solid lines. Note that all residues were fitted together (all temperatures and all magnetic fields) when the 3-site exchange model was used. (D) Populations (U, I in pink; scale on left hand side) and exchange rates (UI = $k_{UI} + k_{IU}$, IF = $k_{IF} + k_{FI}$ in purple; scale on right hand side) as a function of temperature, along with thermodynamic parameters (inset in left corner) for the G48M mutant are shown (middle curve of the three) along with errors of 1 standard deviation. Adapted from Korzhnev et al. [70].

shifts between states I,F($\Delta\omega_{IF}$) and U,F($\Delta\omega_{UF}$) and plateau values for the dispersion curves. Data recorded at five temperatures, ranging from 15 to 35 °C, at spectrometer fields of 500, 600, and 800 MHz and for all residues in the protein with sizeable dispersions, were fit together. The temperature dependence of the extracted populations and rates are shown in Fig. 19D (UI and IF refer to $k_{UI} + k_{IU}$, $k_{IF} + k_{FI}$, respectively). The population of the U state increases from 1 to 5% over the temperature range examined (while the population of I remains at ~1%) with $k_{UI} + k_{IU}$ growing rapidly; this explains why relaxation profiles are better fit to a two-state process at higher temperatures (Fig. 19B). Thermodynamic parameters (G, TS, and H) can be extracted from the temperature dependence of the rates (inset to Fig. 19D). It is thus possible to characterize in some detail the kinetics and thermodynamics of this folding/unfolding reaction.

It is also possible to construct a model for the ensemble of structures that comprise the I state using the ratio $|\Delta\omega_{IF}/\Delta\omega_{UF}|$ and a molecular dynamics protocol that is described elsewhere [70]. Such an analysis shows that strands β2–4 (Fig. 19A) are relatively well defined in the I state, indicating that this region of the protein folds first.

The study described above has also been performed on a second mutant, G48V. An ensemble of structures that describes the I state in this case also shows that β2–4 is well formed. However, the ensemble for G48V is more compact than for G48M, so that the intermediate in the case of G48V may represent a later stage in the folding process [70].

As a final note it should be emphasized that relaxation dispersion experiments make available kinetic, thermodynamic and structural information on 'excited' states that often comprise only a few percent of the total population of molecules in solution and that cannot be observed directly in even the most sensitive NMR experiments. The initial development of these experiments dates back many decades; it seems likely that they will become increasingly important in future biological NMR applications.

4. Concluding remarks

In this review I have attempted to briefly highlight research activities in my laboratory focusing on solution NMR studies of (i) high-molecular-weight proteins and (ii) protein dynamics. It is clear that such studies are still in their early stages. Nevertheless, the rapid development of biomolecular NMR, involving contributions from many research groups, will continue to facilitate future advances and promises to significantly extend the range of applications over those that are currently feasible.

Acknowledgments

References

[1] G. Wider, K. Wüthrich, NMR spectroscopy of large molecules and multimolecular assemblies in solution, Curr. Opin. Struct. Biol. 9 (1999) 594–601.

[2] C. Fernandez, G. Wider, TROSY in NMR studies of the structure and function of large biological macromolecules, Curr. Opin. Struct. Biol. 13 (2003) 570–580.

[3] J. Fiaux, E.B. Bertelsen, A.L. Horwich, K. Wüthrich, NMR analysis of a 900 K GroEL–GroES complex, Nature 418 (2002) 207–221.

[4] G.M. Clore, A.M. Gronenborn, Structures of larger proteins in solution: three- and four-dimensional heteronuclear NMR spectroscopy, Science 252 (1991) 1390–1399.

[5] A. Bax, Weak alignment offers new NMR opportunities to study protein structure and dynamics, Protein Sci 12 (2003) 1–16.

[6] M. Sattler, J. Schleucher, C. Griesinger, Heteronuclear multidimensional NMR experiments for the structure determination of proteins in solution employing pulsed field gradients, Prog. Nucl. Magn. Reson. Spectrosc. 34 (1999) 93–158.

[7] R. Ishima, D.A. Torchia, Protein dynamics from NMR, Nat. Struct. Biol. 7 (2000) 740–743.

[8] R. Bruschweiler, New approaches to the dynamic interpretation and prediction of NMR relaxation data from proteins, Curr. Opin. Struct. Biol. 13 (2003) 175–183.

[9] B.R. Howard, J.A. Endrizzi, S.J. Remington, Crystal structure of *Escherichia coli* malate synthase G complexed with magnesium and glyoxylate at 2.0 Å resolution: mechanistic implications, Biochemistry 39 (2000) 3156–3168.

[10] K. Pervushin, R. Riek, G. Wider, K. Wüthrich, Attenuated T_2 relaxation by mutual cancellation of dipole–dipole coupling and chemical shift anisotropy indicates an avenue to NMR structures of very large biological macromolecules in solution, Proc. Natl. Acad. Sci. USA 94 (1997) 12366–12371.

[11] J.W. Peng, G. Wagner, Investigation of protein motions via relaxation measurements, Methods Enzymol. 239 (1994) 563–596.

[12] V. Tugarinov, P.M. Hwang, L.E. Kay, Nuclear magnetic resonance spectroscopy of high-molecular-weight proteins, Annu. Rev. Biochem. 73 (2004) 107–146.

[13] P.M. Hwang, L.E. Kay, Solution structure and dynamics of integral membrane proteins by NMR: A case study involving the enzyme PagP, Methods Enzymol. (2004) in press.

[14] K.H. Gardner, L.E. Kay, The use of $^2H,^{13}C,^{15}N$ multidimensional NMR to study the structure and dynamics of proteins, Annu. Rev. Biophys. Biomol. Struct. 27 (1998) 357–406.

[15] B.T. Farmer, R.A. Venters, in: N.R. Krishna, L.J. Berliner (Eds.), Biological Magnetic Resonance, Kluwer Academic/Plenum Publishers, New York, 1998, pp. 75–120.

[16] L. Yu, A.M. Petros, A. Schnuchel, P. Zhong, J.M. Severin, K. Walter, T.F. Holzman, S.W. Fesik, Solution structure of an rRNA methyltransferase (ErmAm) that confers MLS antibiotic resistance, Nat. Struct. Biol. 4 (1997) 483–489.

[17] D.C. Williams Jr., M. Cai, G.M. Clore, Molecular basis for synergistic transcriptional activation by Oct1 and Sox2 revealed from the solution structure of the 42-kDa Oct1.Sox2.Hoxb1-DNA ternary transcription factor complex, J. Biol. Chem. 279 (2004) 1449–1457.

[18] V. Tugarinov, R. Muhandiram, A. Ayed, L.E. Kay, Four-dimensional NMR spectroscopy of a 723-residue protein: chemical shift assignments and secondary structure of malate synthase G, J. Am. Chem. Soc. 124 (2002) 10025–10035.

[19] T.M. Larsen, M.M. Benning, G.E. Wesenberg, I. Rayment, G.H. Reed, Ligand-induced domain movement in pyruvate kinase: structure of the enzyme from rabbit muscle with Mg^{2+}, K^+, and L-phospholactate at 2.7 Å resolution, Arch. Biochem. Biophys. 345 (1997) 199–206.

[20] T.M. Larsen, L.T. Laughlin, H.M. Holden, I. Rayment, G.H. Reed, Structure of rabbit muscle pyruvate kinase complexed with Mn^{2+}, K^+, and pyruvate, Biochemistry 33 (1994) 6301–6309.

[21] N. Tjandra, A. Bax, Direct measurement of distances and angles in biomolecules by NMR in a dilute liquid crystalline medium, Science 278 (1997) 1111–1114.

[22] J.H. Prestegard, New techniques in structural NMR—anisotropic interactions, Nat. Struct. Biol. NMR suppl. 5 (1998) 517–522.

[23] V. Tugarinov, L.E. Kay, Quantitative NMR studies of high-molecular-weight proteins: application to domain orientation and ligand binding in the 723 residue enzyme malate synthase G, J. Mol. Biol. 327 (2003) 1121–1133.

[24] M.W. Fischer, J.A. Losonczi, J.L. Weaver, J.H. Prestegard, Domain orientation and dynamics in multidomain proteins from residual dipolar couplings, Biochemistry 38 (1999) 9013–9022.

[25] N.R. Skrynnikov, N.K. Goto, D. Yang, W.Y. Choy, J.R. Tolman, G.A. Mueller, L.E. Kay, Orienting domains in proteins using dipolar couplings measured by liquid-state NMR: differences in solution and crystal forms of maltodextrin binding protein loaded with β-cyclodextrin, J. Mol. Biol. 295 (2000) 1265–1273.

[26] K. Wüthrich, NMR of Proteins and Nucleic Acids, John Wiley, New York, 1986.

[27] K.H. Gardner, L.E. Kay, Production and incorporation of $^{15}N,^{13}C,^2H$ (^1H-δ1 methyl) isoleucine into proteins for

multidimensional NMR studies, J. Am. Chem. Soc. 119 (1997) 7599–7600.

[28] N.K. Goto, K.H. Gardner, G.A. Mueller, R.C. Willis, L.E. Kay, A robust and cost-effective method for the production of Val, Leu, Ile (δ 1) methyl-protonated ^{15}N-,^{13}C-,^{2}H-labeled proteins, J. Biomol. NMR 13 (1999) 369–374.

[29] V. Tugarinov, L.E. Kay, Ile, Leu, and Val methyl assignments of the 723-residue malate synthase G using a new labeling strategy and novel NMR methods, J. Am. Chem. Soc. 125 (2003) 13868–13878.

[30] V. Tugarinov, L.E. Kay, Side chain assignments of Ile delta 1 methyl groups in high-molecular-weight proteins: an application to a 46 ns tumbling molecule, J. Am. Chem. Soc. 125 (2003) 5701–5706.

[31] L.G. Werbelow, A.G. Marshall, Internal rotation and nonexponential methyl nuclear relaxation for macromolecules, J. Magn. Reson. 11 (1973) 299–313.

[32] L.G. Werbelow, D.M. Grant, Intramolecular dipolar relaxation in multispin systems, Adv. Magn. Reson. 9 (1977) 189–299.

[33] N. Muller, G. Bodenhausen, R.R. Ernst, Relaxation-induced violations of coherence transfer selection rules in nuclear magnetic resonance, J. Magn. Reson 75 (1987) 297–334.

[34] L.E. Kay, T.E. Bull, Heteronuclear transverse relaxation in AMX, AX_2, and AX_3 spin systems, J. Magn. Reson. 99 (1992) 615–622.

[35] L.E. Kay, D.A. Torchia, The effects of dipolar cross-correlation on ^{13}C methyl-carbon T_1, T_2 and NOE measurements in macromolecules, J. Magn. Reson. 95 (1991) 536–547.

[36] V. Tugarinov, P. Hwang, J. Ollerenshaw, L.E. Kay, Cross-correlated relaxation enhanced ^{1}H–^{13}C NMR spectroscopy of methyl groups in very high-molecular-weight proteins and protein complexes, J. Am. Chem. Soc. 125 (2003) 10420–10428.

[37] L. Mueller, Sensitivity enhanced detection of weak nuclei using heteronuclear multiple quantum coherence, J. Am. Chem. Soc. 101 (1979) 4481–4484.

[38] A. Bax, R.H. Griffey, B.L. Hawkings, Correlation of proton and nitrogen-15 chemical shifts by multiple quantum NMR, J. Magn. Reson. 55 (1983) 301–315.

[39] G. Bodenhausen, D.J. Rubin, Natural abundance nitrogen-15 NMR by enhanced heteronuclear spectroscopy, Chem. Phys. Lett. 69 (1980) 185–189.

[40] V. Tugarinov, L.E. Kay, An isotope labeling strategy for methyl-TROSY spectroscopy, J. Biomol. NMR 28 (2004) 165–172.

[41] V. Tugarinov, R. Sprangers, L.E. Kay, Line narrowing in methyl-TROSY using zero-quantum ^{1}H–^{13}C NMR spectroscopy, J. Am. Chem. Soc. 126 (2004) 4921–4925.

[42] V. Tugarinov, L.E. Kay, Stereospecific NMR assignments of prochiral methyls, rotameric states and dynamics of valine residues in malate synthase G, J. Am. Chem. Soc. 126 (2004) 9827–9836.

[43] A. Bax, G.W. Vuister, S. Grzesiek, F. Delaglio, A.C. Wang, R. Tschudin, G. Zhu, Measurement of homo- and heteronuclear *J* couplings from quantitative *J* correlation, Methods Enzymol. 239 (1994) 79–105.

[44] D.M. Korzhnev, K. Kloiber, V. Kanelis, V. Tugarinov, L.E. Kay, Probing slow dynamics in high-molecular-weight proteins by methyl-TROSY NMR spectroscopy: application to a 723-residue enzyme, J. Am. Chem. Soc. 126 (2004) 3964–3973.

[45] V.Y. Orekhov, I.V. Ibraghimov, M. Billeter, MUNIN: a new approach to multidimensional NMR spectra interpretation, J. Biomol. NMR 20 (2001) 49–60.

[46] L.E. Kay, D.A. Torchia, A. Bax, Backbone dynamics of proteins as studied by ^{15}N inverse detected heteronuclear NMR spectroscopy: application to staphylococcal nuclease, Biochemistry 28 (1989) 8972–8979.

[47] J.W. Peng, G. Wagner, Mapping of spectral density functions using heteronuclear NMR relaxation measurements, J. Magn. Reson. 98 (1992) 308–332.

[48] L.E. Kay, T.E. Bull, L.K. Nicholson, C. Griesinger, H. Schwalbe, A. Bax, D.A. Torchia, The measurement of heteronuclear transverse relaxation times in AX3 spin systems via polarization transfer techniques, J. Magn. Reson. 100 (1992) 538–558.

[49] A. Abragam, Principles of Nuclear Magnetism, Clarendon Press, Oxford, 1961.

[50] D.R. Muhandiram, T. Yamazaki, B.D. Sykes, L.E. Kay, Measurement of deuterium T_1 and $T_{1\rho}$ relaxation times in uniformly ^{13}C labeled and fractionally deuterium labeled proteins in solution, J. Am. Chem. Soc. 117 (1995) 11536–11544.

[51] O. Millet, D.R. Muhandiram, N.R. Skrynnikov, L.E. Kay, Deuterium spin probes of side-chain dynamics in proteins. 1. Measurement of five relaxation rates per deuteron in C-13-labeled and fractionally H-2-enriched proteins in solution, J. Am. Chem. Soc. 124 (2002) 6439–6448.

[52] N.R. Skrynnikov, O. Millet, L.E. Kay, Deuterium spin probes of side-chain dynamics in proteins. 2. Spectral density mapping and identification of nanosecond time-scale side-chain motions, J. Am. Chem. Soc. 124 (2002) 6449–6460.

[53] J.P. Jacobsen, H.K. Bildsoe, K. Schaumburg, Application of density of matrix formalism in NMR spectroscopy. II. The one-spin-1 case in anisotropic phase, J. Magn. Reson. 23 (1976) 153–164.

[54] L.E. Kay, D.R. Muhandiram, G. Wolf, S.E. Shoelson, J.D. Forman-Kay, Correlation between binding and dynamics at SH2 domain interfaces, Nat. Struct. Biol. 5 (1998) 156–163.

[55] A.L. Lee, S.A. Kinnear, A.J. Wand, Redistribution and loss of side chain entropy upon formation of a calmodulin–peptide complex, Nat. Struct. Biol. 7 (2000) 72–77.

[56] W.Y. Choy, D. Shortle, L.E. Kay, Side chain dynamics in unfolded protein states: an NMR based ^{2}H spin relaxation study of $\Delta131\Delta$, J. Am. Chem. Soc. 125 (2003) 1748–1758.

[57] A.L. Lee, A.J. Wand, Microscopic origins of entropy, heat capacity and the glass transition in proteins, Nature 411 (2001) 501–504.

[58] A. Mittermaier, L.E. Kay, The response of internal dynamics to hydrophobic core mutations in the SH3 domain from the Fyn tyrosine kinase, Protein Sci. 13 (2004) 1088–1099.

[59] E.C. Johnson, T.M. Handel, Effect of hydrophobic core packing on side chain dynamics, J. Biomol. NMR 15 (1999) 135–143.

[60] P.M. Hwang, W.Y. Choy, E.I. Lo, L. Chen, J.D. Forman-Kay, C.R. Raetz, G.G. Prive, R.E. Bishop, L.E. Kay, Solution structure and dynamics of the outer membrane enzyme PagP by NMR, Proc. Natl. Acad. Sci. USA 99 (2002) 13560–13565.

[61] P.M. Hwang, R.E. Bishop, L.E. Kay, The integral membrane enzyme PagP alternates between two dynamically distinct states, Proc. Natl. Acad. Sci. USA 101 (2004) 9618–9623.

[62] R.E. Bishop, H.S. Gibbons, T. Guina, M.S. Trent, S.I. Miller, C.R. Raetz, Transfer of palmitate from phospholipids to lipid A in outer membranes of gram-negative bacteria, EMBO J. 19 (2000) 5071–5080.

[63] V. Ahn, E.I. Lo, C.K. Engel, L. Chen, L.E. Kay, R.E. Bishop, G.G. Prive, A hydrocarbon ruler measures palmitate in the enzymatic acylation of endotoxin, EMBO J. 23 (2004) 2931–2941.

[64] N.A. Farrow, O. Zhang, J.D. Forman-Kay, L.E. Kay, A heteronuclear correlation experiment for simultaneous determination of ^{15}N longitudinal decay and chemical exchange rates of systems in slow equilibrium, J. Biomol. NMR 4 (1994) 727–734.

[65] A.G. Palmer, C.D. Kroenke, J.P. Loria, NMR methods for quantifying microsecond-to-millisecond motions in biological macromolecules, Methods Enzymol. 339 (2001) 204–238.

[66] A. Fersht, Structure and Mechanism in Protein Science, W.H. Freeman, New York, 1999.

[67] Y.W. Bai, T.R. Sosnick, L. Mayne, S.W. Englander, Protein-folding intermediates-native-state hydrogen-exchange, Science 269 (1995) 192–197.

[68] O. Zhang, J.D. Forman-Kay, Structural characterization of folded and unfolded states of an SH3 domain in equilibrium in aqueous buffer, Biochemistry 34 (1995) 6784–6794.

[69] A.A. Di Nardo, D.M. Korzhnev, P.J. Stogios, A. Zarrine-Afsar, L.E. Kay, A.R. Davidson, Dramatic acceleration of protein folding by stabilization of a nonnative backbone conformation, Proc. Natl. Acad. Sci. USA 101 (2004) 7954–7959.

[70] D.M. Korzhnev, X. Salvatella, M. Vendruscolo, A.A. Di Nardo, A.R. Davidson, C.M. Dobson, L.E. Kay, Low-populated folding intermediates of Fyn SH3 characterized by relaxation dispersion NMR, Nature 430 (2004) 586–590.

[71] M.E. Noble, A. Musacchio, M. Saraste, S.A. Courtneidge, R.K. Wierenga, Crystal structure of the SH3 domain in human Fyn; comparison of the three-dimensional structures of SH3 domains in tyrosine kinases and spectrin, EMBO J. 12 (1993) 2617–2624.

[72] S. Vijay-Kumar, C.E. Bugg, W.J. Cook, Structure of ubiquitin refined at 1.8 angstroms resolution, J. Mol. Biol. 194 (1987) 531–544.

[73] D.W. Heinz, W.A. Baase, F.W. Dahlquist, B.W. Matthews, How amino-acid insertions are allowed in an alpha-helix of T4 lysozyme, Nature 361 (1993) 561–564.

[74] C.W. Muller, G.E. Schulz, Structure of the complex between adenylate kinase from *Escherichia coli* and the inhibitor Ap5A refined at 1.9 Å resolution. A model for a catalytic transition state, J. Mol. Biol. 224 (1992) 159–177.

[75] A.J. Sharff, L.E. Rodseth, F.A. Quiocho, Refined 1.8-Å structure reveals the mode of binding of β-cyclodextrin to the maltodextrin binding protein, Biochemistry 32 (1993) 10553–10559.